Metabolism regulates exposure of pancreatic islets to circulating molecules in vivo

Michau, Aurélien; Hodson, David; Fontanaud, Pierre; Guillou, Anne; Espinosa-Carrasco, Gabriel; Molino, François; Peters, Catherine J; Robinson, Iain C; Le Tissier, Paul; Mollard, Patrice; Schaeffer, Marie

DOI:
10.2337/db15-1168

License:
Other (please specify with Rights Statement)

Document Version
Peer reviewed version

Citation for published version (Harvard):
Michau, A, Hodson, DJ, Fontanaud, P, Guillou, A, Espinosa-Carrasco, G, Molino, F, Peters, CJ, Robinson, IC, Le Tissier, P, Mollard, P & Schaeffer, M 2015, 'Metabolism regulates exposure of pancreatic islets to circulating molecules in vivo', Diabetes. https://doi.org/10.2337/db15-1168

Metabolism regulates exposure of pancreatic islets to circulating molecules *in vivo*

[1,2,3*]Aurélien Michau, [1,2,3,4,5*]David J. Hodson, [1,2,3]Pierre Fontanaud, [1,2,3]Anne Guillou, [1,2,3,6]Gabriel Espinosa-Carrasco, [1,2,3,7]François Molino, [8,9]Catherine J. Peters, [8]Iain C. Robinson, [10]Paul Le Tissier, [1,2,3]Patrice Mollard, [1,2,3§]Marie Schaeffer

[1]CNRS, UMR-5203, Institut de Génomique Fonctionnelle, F-34000 Montpellier, France; [2]INSERM, U1191, F-34000 Montpellier, France; [3]University of Montpellier, F-34000 Montpellier, France;

[4]Section of Cell Biology and Functional Genomics, Department of Medicine, Imperial College London, Imperial Centre for Translational and Experimental Medicine, Hammersmith Hospital, Du Cane Road, London W12 0NN, UK;

[5]Institute of Metabolism and Systems Research (IMSR), University of Birmingham, Birmingham B15 2TT, UK;

[6]Institute for Regenerative Medicine and Biotherapy, U1183, Lymphocyte differentiation, tolerance and metabolism laboratory, F-34295, Montpellier, France;

[7]University of Montpellier, CNRS, UMR-5221, Charles Coulomb Laboratory, F-34095 Montpellier, France;

[8]National Institute for Medical Research, Division of Molecular Neuroendocrinology, London, NW7 1AA, UK;

[9]Current address: Department of Endocrinology, Great Ormond Street Hospital for Children, London WC1N 3JH, UK;

[10]Centre for Integrative Physiology, University of Edinburgh, Edinburgh, EH8 9XD, UK;

[*]Equal contributions

Diabetes Publish Ahead of Print, published online November 18, 2015

§Correspondence: Dr. Marie Schaeffer, Department of Endocrinology, Institute of Functional Genomics, Montpellier 34094, France

Fax: +33434359292

Marie.Schaeffer@igf.cnrs.fr

Running title: *in vivo* vessel permeability in pancreatic islets

Keywords: beta cell, vessel, permeability, gestation, high fat diet, proliferation, imaging, in vivo, diffusion.

Abbreviations: T2D: type 2 diabetes, HFD: high fat diet, RIP: rat insulin promoter, IPGTT: intra-peritoneal glucose tolerance test, SD: standard diet, TRP: tryptophan

ABSTRACT

Pancreatic beta cells modulate insulin secretion through rapid sensing of blood glucose and integration of gut-derived signals. Increased insulin demand during pregnancy and obesity alters islet function and mass, and leads to gestational and type 2 diabetes in predisposed individuals. However, it is unclear how blood-borne factors dynamically access the islets of Langerhans. Thus, understanding the changes in circulating molecule distribution that accompany compensatory beta cell expansion may be key to developing novel anti-diabetic therapies. Here, using 2-photon microscopy *in vivo* in mice, we demonstrate that islets are almost instantly exposed to peaks of circulating molecules, which rapidly pervade the tissue before clearance. In addition, both gestation and short-term high fat diet-feeding decrease molecule extravasation and uptake rates *in vivo* in islets, independently of beta cell expansion or islet blood flow velocity. Together, these data support a role for islet vascular permeability in shaping beta cell adaptive responses to metabolic demand by modulating the access and sensing of circulating molecules.

INTRODUCTION

Islets of Langerhans in adult mice are primarily composed of insulin-producing beta cells (up to 90%), surrounded by other endocrine cell types [1], and serve to maintain whole body glucose homeostasis. Islets are organized in clusters distributed preferentially along large blood vessels [2], and the resident endocrine cells are interwoven with a dense capillary network. Islet capillaries are denser, more tortuous and more fenestrated than vessels of the surrounding exocrine tissue [3]. In addition, relative to their total mass (~1% of the pancreas), islets are highly perfused (~10% of pancreatic blood flow) [4, 5]. Both these traits are critical to ensure adequate oxygen and nutrient supply, as well as fast-sensing of circulating molecules and rapid hormone transport into the blood. Although beta cells integrate a range of signals from the circulation involved in insulin secretion and/or beta cell function, survival and proliferation (glucagon-like peptide-1 (GLP-1), prolactin/placental lactogen) [6–8], the access dynamics of circulating molecules to islets remain largely unexplored.

While adult beta cells are terminally differentiated with low proliferative capacity, conditions of increased insulin demand such as pregnancy and obesity can profoundly alter beta cell function and/or mass [9]. Failure to compensate for increased insulin demand contributes to gestational diabetes and type 2 diabetes (T2D) in genetically-predisposed individuals [10]. Beta cell adaption during gestation and high fat diet (HFD) is widely studied [11–15], and vessel properties are modified during these highly-proliferative phases. For instance, islet blood flow varies during acute and chronic blood glucose concentration changes [4, 16–18], insulin resistance states [19], and pregnancy in the rat [20]. Highlighting the importance of islet blood flow in beta cell function, ablation of endothelial insulin signaling impairs insulin release through effects on the pancreatic blood circulation [21].

However, whether islet vascular permeability is also affected by altered metabolism remains uncharacterized. Understanding the changes in molecule access and distribution that accompany compensatory beta cell expansion may be key to developing novel anti-diabetic therapies/strategies. Therefore, using *in vivo* imaging approaches, we examined whether alterations in islet vascular permeability are associated with beta cell adaptation to both physiological and pathological metabolic triggers.

RESEARCH DESIGN AND METHODS

Mice and *in vivo* surgery

All animal studies were approved by the Languedoc Roussillon Institutional Animal Care and Use Committee (CEEA-LR-1053). Virgin or G14.5 gestating 9-12 weeks old female C57BL/6J mice were used. All experiments were performed on animals fed ad-libitum. In some experiments, virgin RIPTVA-mCherry mice, produced at the National Institute of Medical Research, London, were used to facilitate localization of islets. The construct used to produce these mice contained 0.7kb RIP (Rat Insulin Promoter) sequence upstream of TVA-IRES-mCherry gene, followed by the 3'UTR of the rat prolactin gene (hGH minigene was not used) [22, 23], and was micro-injected into the pronucleus of fertilized oocytes of super-ovulated (CBA/Ca × C57BL/10)F1 mice. RIPTVA-mCherry mice obtained were back-crossed to C57BL/6J mice for > 8 generations. Mice were either placed on standard diet (SD), tryptophan +/- diets (0/0.18% TRP), or high fat diet (63% calories from fat) (Safe Diets). In some cases, virgin animals fed 2 weeks with SD were used as controls for G14.5 and 2 weeks HFD-fed animals. Intra-peritoneal glucose tolerance tests (IPGTT) and glucose-stimulated insulin secretion tests were as described [21, 24]. For *in vivo* imaging, the pancreas was exteriorized by surgery. Animals were anesthetized by injection of ketamine/xylazine (0.1/0.02 mg/g), and temperature controlled as described [25, 26]. Respiration was controlled by tracheotomy. An incision was made in the peritoneum and the pancreas was gently maneuvered onto a custom-made metallic stage covered with a 2 mm-thick layer of soft polymer (Bluesil). The pancreas was pinned to the polymer using 4-5 stainless steel minutien insect pins (tip = 0.0125 mm). To prevent desiccation, the tissue was superfused with a NaCl 0.9% heated to 37°C. Imaging commenced 30-40 min post-anesthesia.

Measurements of *in vivo* molecule extravasation rate and diffusion in tissue

Molecule extravasation was imaged using a multiphoton microscope (Zeiss 7MP) adapted with a long-working distance objective M Plan Apo NIR ×20, 0.4 NA (Mitutoyo), and multiphoton excitation and emitted fluorescence collection were as described [26]. Surface islets were identified through mCherry localization or by light contrast. FITC- or rhodamine-labeled dextrans (Sigma) (25 mg/ml in NaCl 0.9%, 100µl/20 g body weight) were injected through a jugular catheter. In some experiments, 100µl/20 g body weight of 50 mg/ml dextran was used. As this had no effect on measurements, data were pooled. Recordings in islets, distinguishable by their tortuous vessels, at depths of 15 to 40 µm below the surface, were started at the time of injection, and acquisition rate was set to 3.5 frames/s. Regions of interest (ROI) in vessels and in the directly adjacent parenchyma were selected in each movie (3-4 µm diameter circles). At least 4 movies from 4 different mice were analyzed per molecular weight and condition.

Tissue movement was corrected using a registration tool based on a subpixel translation obtained from a minimal image difference search, as previously described [25, 26]. Briefly, movies were imported into ImageJ (NIH) and the average distance of each frame calculated versus a reference image over eight trials. A translation was then performed corresponding to the minimum of a parabolic interpolation, before application to the entire image stack. To obtain the extravasation rate value p (µm/s) for each molecule, an automated routine programmed in MATLAB R2011a software was used [26]. This is described mathematically as $\frac{\partial \Phi}{\partial t} = -D\Delta\Phi + p\nabla\Phi.$ $\nabla\Phi$, corresponding to the fluorescence gradient in μm^{-1} and equals $\frac{\Phi_{inside}(t) - \Phi_{outside}(t)}{l}$, where $\Phi_{inside} - \Phi_{outside}$ is the measured difference between fluorescence intensities in the vessel and the parenchyma, and l is half the distance

between the ROIs in μm. D corresponds to the diffusion coefficient in $\mu m^2/s$, p is the extravasation rate in μm/s, and $D\Delta\Phi$ corresponds to the diffusion term. The ascending phase of the fluorescence profile obtained experimentally in the vessel ROI was used as input to the model. Then, the value of p for which the simulated profile of fluorescence intensity increase in the parenchyma over time best fitted experimental values, was selected. The decreasing phase of the fluorescence profiles in selected ROIs were modeled using the Nelder-Mead Method optimization algorithm, consisting of a decreasing exponential function (MATLAB), before calculation of fluorescence decay rates (s^{-1}), corresponding to the time constant ($1/\tau$) of the exponential fluorescence decay ($f(x) = e^{(-t/\tau)}$).

Measurements of *in vivo* 2-NBDG uptake rate

2-NBDG (2-(*N*-(7-Nitrobenz-2-oxa-1,3-diazol-4-yl)Amino)-2-Deoxyglucose) (Life Technologies) was injected either 5 mg/kg i.v., or 10 mg/kg i.m., in 100 μl, or 40 μl of 0.9% NaCl, respectively. Although plasma volume increases during gestation in mice (~ 26%) [27], this is in accordance with a similar increase in weight (~ 24%), justifying a mg/kg correction. Furthermore, uptake rates were unchanged when 2-NBDG was injected above 4 mg/kg i.v. or 6.25 mg/kg i.m. Vessels were labeled with fluorescent dextran to facilitate islet localization. Multiphoton excitation was delivered at 890 nm. Each z plane was scanned every 15s (120 μm stacks). Movies were stabilized using Huygens Essential (SVI). Fluorescence increase over time in ROIs was measured. Following i.v. injection, the first 1.5 min of recordings were excluded from analysis, due to contamination of signal by molecules diffusing out of vessels. Background fluorescence in exocrine tissue was subtracted from signal measured in islets, and fluorescence measurements were normalized. Uptake of 2-NBDG was modeled using either a one-phase association curve (i.v), or a variable slope sigmoidal curve (i.m.). First derivatives

of the modeled sigmoidal curves were generated using GraphPad Prism. Vmax of derivatives, and inflexion points of sigmoidal and one-phase association curves were compared.

Measurements of red blood cells velocity *in vivo*

Blood cells velocity was measured using an epi-fluorescence stereomicroscope (StereoDiscovery, Carl Zeiss), as described [25]. Mice were anesthetized using ketamine/xylazine (0.1/0.02 mg/g) i.p. Plasma was labeled with FITC-150 kDa dextran. Fluorescence emission was captured using an ORCA Flash4.0 sCmos (Hamamatsu). Acquisition rate was 150 frames/s, > 1000 frames per movie were captured. Velocities were obtained by analyzing diagrams of the intensities along defined capillary paths (in ImageJ [25]). Five to 6 mice per condition, and 2-9 islets per mouse were analyzed.

Confocal imaging

Pancreata were fixed overnight in 4% paraformaldehyde, before head-to-tail slicing on a Leica vibratome (100 µm), or snap-frozen in OCT and sectioned using a cryostat (20 µm). In some experiments, vessels were filled using gelatin (Sigma) labeled with FITC, through intra-cardiac perfusion [25]. Antibody labeling was as described [26]. Images were acquired using a Zeiss LSM 780 confocal microscope. Images were analyzed using Imaris (Bitplane), Volocity (Perkin Elmer) and ImageJ (NIH).

For quantifications, one to four slices were randomly selected from at least six animals/group, and all islets present analyzed, corresponding to minimum 15 islets/mouse. *A priori*, this is sufficiently-powered to detect a minimum 1.2-fold difference with a SD of 40%, a power of 0.9, and alpha = 0.05 (G*Power 3.1). Beta cell proliferation was measured on slices stained for Ki67 (rabbit, 1:200, CliniSciences), insulin (guinea-pig, 1:400, Abcam) and dapi (Sigma). The proportion of proliferative beta cells was obtained by dividing number of Ki67+ nuclei by total number of nuclei of insulin+ cells in islets, as described [14]. Vessel

density in z-stack images was assessed by calculating vessel (gelatin-FITC labeled or rat anti-CD31, 1:100, BD Pharmingen) and islet (insulin+ or mCherry) volume using Volocity (Perkin Elmer). To determine beta cell size, pancreas slices were stained for insulin, E-cadherin (rat, 1:500, Takara) and dapi. The cross-sectional area of E-cadherin insulin-positive cells in which a cut nuclei was present was measured using ImageJ (NIH), as described [28].

Electron microscopy

Pancreata were collected and fixed in 4% paraformaldehyde, 2.5% glutaraldehyde at 4°C, and sliced on a Leica vibratome. Unlabeled slices were treated as described [29]. Images were acquired on a transmission electron microscope (Hitachi H-7100). Density of fenestrae per μm was obtained by counting fenestrae on available endothelium of individual vessels after subtraction of the perikaryal length. Internal fenestrae diameters and islet vessel lumen perimeters in vessels present in cross sections were manually measured using ImageJ (NIH).

Statistical analysis

Values are represented as means ± SEM, and tests were performed using GraphPad Prism. Normality was assessed using D'Agostino-Pearson test. Comparisons were made using either unpaired Student's t-test, or two-tailed Mann-Whitney U-test, as appropriate. Multiple comparisons were made using one-way ANOVA followed by Bonferroni's post-hoc test, or two-way ANOVA using Turkey's multiple comparison test. P values were considered significant at $P<0.05$*, 0.01**, 0.001***.

RESULTS

In vivo permeability of vessels in pancreatic islets

To study molecule access in islets, we developed a novel approach to image the pancreas directly *in vivo* in anesthetized mice, using a 2-photon microscope adapted with long working-distance objectives [26] (Fig. 1A-B). Islet localization was initially facilitated by using mice on a C57BL/6J background expressing mCherry under the control of the rat insulin promoter (RIP) (Fig. S1). As no difference with wild-type C57BL/6J mice were observed, data were pooled. Fluorescent-dextran was used for extravasation rate measurements, since it avoids artefacts introduced by receptor binding and/or uptake by cells. Injection of FITC-labeled dextran (MW <70 kDa) into the jugular vein of virgin animals induced a steep increase followed by a rapid decrease in intra-islet fluorescence, suggesting that beta cells are only briefly exposed to circulating molecule (Fig. 1C-D, movie S1). Extravasation rates from endocrine capillaries were significantly greater than from the surrounding exocrine vessels (~5-fold for 4 and 10 kDa molecules and ~10-fold for 20 and 40 kDa) (Fig. 1E), as expected from the reported differences in fenestration density [3]. In the islets, molecules smaller than 70 kDa diffused rapidly across capillaries (Fig. 1E, movie S1). By contrast, diffusion of 20 to 40 kDa molecules in the exocrine tissue was very slow, albeit detectable.

In addition to molecule access to pancreatic tissue, we also assessed molecule retention in the extracellular space subsequent to entry. To measure this, fluorescence exponential decay rates in tissue were calculated. In virgin animals, small molecules (~4 kDa) diffused rapidly out of both exocrine and endocrine tissues, whereas for larger molecules (~10

kDa), diffusion occurred more slowly out of the exocrine compartment (Fig. 1F). This finding supports the notion that endocrine cells only very briefly encounter extravasating molecules.

Islet vessel permeability is modified by metabolic demand

We next sought to investigate if islet vessel permeability was modified in response to changes in metabolic demand. First, gestation was chosen as it represents a normal physiological state of insulin resistance accompanied by changes in beta cell proliferation and function [11, 30]. As expected, islets from G14.5 animals were 2.5-fold larger than in virgins, and this was associated with beta cell hypertrophy/hyper-proliferation, increased basal insulinemia, and unchanged glucose-stimulated insulin secretion (Fig. 2A-G, Fig. S2). As evidenced by intra-peritoneal glucose tolerance testing (IPGTT), G14.5 mice were glucose intolerant (Fig. 2H-I). Second, to determine whether adaptive changes in the islet vasculature were specifically associated with pregnancy, or reflected a more generalized response to short-term metabolic stress, virgin female mice were fed high fat diet (HFD) for two weeks. This paradigm has the advantage of preventing the hormonal changes occurring during gestation. As anticipated [13–15], animals fed HFD were heavier and more glucose intolerant than their standard chow-fed counterparts, while basal and glucose-stimulated insulin secretion were not significantly modified (Fig. 3A-E). Although an increase in islet size could not yet be observed at this stage (Fig. 3F-G), beta cells were hypertrophic (Fig. 3H), and an increase in beta cell proliferation was evident, as measured by the proportion of Ki67 positive beta cells (2-fold increase compared to SD-fed mice) (Fig. 3I-J), and reported in [14].

At G14.5, although the general shape of the permeability curve and molecule size cut-off remained unchanged, molecule extravasation rates from the islet vasculature were significantly decreased (Fig. 4A-B, movie S2). This effect was particularly marked for 10 and 20 kDa molecules and was specific to islets, since no alteration could be detected in exocrine

vessels (Fig. 4B). In addition, there was an increase in the rate of molecule diffusion out of the endocrine tissue compared to virgin animals (Fig. 4C). Similarly to G14.5, a significant decrease in molecule extravasation rate was present in islets of HFD-fed mice, and this was more pronounced for smaller molecule sizes (Fig. 4D-E, movie S3). In addition, fluorescence decay rates in the endocrine tissue of HFD-fed animals were comparable to those measured at G14.5 (Fig. 4F). Decreased retention would shorten the already short-lived peak of molecule in the tissue. Thus, beta cells unexpectedly experience less exposure to circulating molecules during acute metabolic demand induced by pregnancy and HFD.

Islet structural changes accompanying altered permeability

Next, to investigate potential mechanisms involved in modifications to islet vessel permeability, relevant structural vascular parameters were assessed. At G14.5, there was a striking increase in islet volume occupied by capillaries (Fig. 5A), consistent with the reported increase in islet endothelial proliferation during gestation [30]. By contrast to the effects of long-term high-fat feeding (Fig. S3), and described in [19], changes in vessel density were absent following 2 weeks of HFD (Fig. 5B). As an increase in islet vessel volume can result from dilation and/or angiogenesis [19], we measured lumen perimeters in cross sections using electron microscopy. Mean islet vessel perimeter was significantly increased in gestating animals (Fig. 5C-D). While most vessels were a similar size to virgin animals, some appeared dilated (Fig. 5D). By contrast, the reported long-term effects of HFD on vessels dilation [19] (Fig. S3) were not evident after 2 weeks of treatment (Fig. 5C, E). Fenestration density and mean fenestrae diameter remained unchanged between both virgin and G14.5 animals, and SD and HFD-fed animals (~75 nm in both cases) (Fig. 5F-K).

Cell proliferation does not modify islet permeability

A common feature of both gestation and HFD treatment is beta cell expansion [14, 11]. To test whether cell proliferation could drive modifications in vascular permeability, the compensatory increases in beta cell mass during gestation were prevented by feeding animals from G8.5 to G14.5 with a tryptophan deficient diet (TRP- diet), thereby inhibiting serotonin synthesis [31]. Both virgin and gestating mice fed with TRP- diet for 6 days lost weight (Fig. 6A), but only gestating mice became glucose intolerant (Fig. 6B-C). No increase in islet size or beta cell proliferation could be observed at G14.5 compared to virgin animals (Fig. 6D-G), as expected [31]. However, extravasation rates of molecules were still reduced in gestating animals fed with TRP- diet (Fig. 6H-I and movie S4). Remarkably, in both virgin and G14.5 TRP- diet-fed mice, values obtained were similar to those of animals fed standard chow, despite the absence of gestational increases in islet size. However, islet size distribution and beta cell density in islets were altered at G14.5 (Fig. S4A-C), and other changes induced by gestation were still present, including beta cell hypertrophy, and increased islet volume occupied by vessels (Fig. S4D-F). Fenestrae diameters and density remained unchanged (Fig. S4G-H). These findings suggest that changes in islet vessels permeability during gestation are independent of beta cell proliferation.

Islet glucose uptake *in vivo* is decreased in response to metabolic stressors

Extravasation and retention of molecules may conceivably be modified by binding and uptake kinetics, questioning whether islets actually experience 'lesser exposure' to circulating bioactive molecules. To examine this, glucose uptake was tracked directly *in vivo* in islets using 2-NBDG. This 'trappable' fluorescent glucose analog was either injected intramuscularly to mimic an increase in molecule concentration in the periphery (e.g. glucose release, GLP-1 secretion), or intravenously to control for effects of peripheral glucose transport on islet fluorescence accumulation (Fig. 7, movies S5 and S6). Islet fluorescence

increase followed sigmoidal or one-phase association curves in response to i.m. (Fig. 7A-B), or i.v. injection (Fig. 7C-D), respectively. Comparison of fitted curves versus virgin mice revealed, for both injection regimes, reduced 2-NBDG incorporation rates during gestation (G14.5) and HFD-feeding, with effects noticeably more pronounced in the latter. Thus, metabolic stressors impinge upon substrate uptake, and this occurs in a direction which strengthens a role for permeability in islet function through delayed exposure to circulating molecules.

Islet blood flow *in vivo* is unchanged by acute increases in metabolic demand

Although the method used to calculate extravasation rate of molecule is independent of vascular flow, 2-NBDG binding rate could conceivably be affected by changes in islet blood flow velocity. To assess the relative importance of blood flow dynamics, we measured red blood cell velocity *in vivo*, and found that it was comparable in both the endocrine and exocrine compartments in virgin, G14.5 and 2 weeks HFD-fed animals (Fig. 8A-B, movie S7). Consistent with that previously reported [18], exocrine and islet blood flow under hyperglycemia did not significantly differ (Fig. 8B-C). In addition, anesthesia-induced hyperglycemia [32] was similar under all conditions examined (Fig. 8C). Thus, delayed 2-NBDG uptake rate during increased metabolic demand is unlikely to be a consequence of reduced islet blood flow.

DISCUSSION

T2D can be described as a failure of beta cells to compensate for peripheral insulin resistance, leading to glucose intolerance and health complications [33]. While most studies have understandably focused upon impaired beta cell function and insulin receptor signaling, the islet microenvironment may provide another route for defective insulin secretion during T2D. We therefore aimed to study the access of circulating molecules to islets under normal conditions, as well as during both physiological (pregnancy) and pathological (HFD) increased metabolic demands. Using *in vivo* 2-photon microscopy applied to the pancreas of anaesthetized mice, we found that beta cells fleetingly encounter circulating molecules, which rapidly pervades the tissue before clearance, and that both gestation and short-term HFD (2 weeks) induce decreases in islet vascular permeability and molecule retention. Vascular permeability remained reduced following prevention of gestation-induced beta cell mass expansion, suggesting that cell proliferation is unlikely to be a primary driver of islet vascular changes. Divergent effects of gestation and 2 weeks HFD were observed on islet vessel dilation, suggesting that different mechanisms may be involved in the regulation of microenvironment properties. Nonetheless, altered molecule access dynamics and lowered exposure to circulating molecule were unifying features of both paradigms. A summary of results is presented in Table S1.

The circulation of molecules within the intercellular microenvironment is dependent on tissue properties and can greatly influence the sensing of blood-borne signals, in addition

to downstream tissue responses [34]. By tracking events *in vivo* in real-time, we were able to determine that circulating molecules (< 70 kDa) could rapidly diffuse through the highly-fenestrated capillaries of islets, similar to that described in other fenestrated vascular beds *in vivo* [26]. In the pancreas, fenestration density greatly influences molecule extravasation, as evidenced by the divergence in rates between exocrine and endocrine tissue, the former irrigated by less fenestrated capillaries [3]. Given the density of vascularization in islets, and the direct proximity of each beta cell to a vessel, this result strongly suggests that beta cells are capable of almost immediately (< 1s) sensing a peak in circulating molecule. Incidentally, beta cells are capable of responding to stimuli delivered over similar time courses [35, 36]. This finding has important implications for access of factors secreted in a pulsatile manner in distant body compartments and involved in beta cell function and/or insulin secretion (e.g. GLP-1, 3.2 kDa; prolactin/placental lactogen, 22 kDa).

By finely regulating the distribution of incoming and outgoing factors through their storage/segregation, the tissue microenvironment plays an important role in molecule action. For example, various niches which favor cell proliferation have been identified, and this may be linked to particular properties of the tissue or presence of growth factors [37, 38]. In virgin animals, small molecules such as 4 kDa dextran diffused equally rapidly out of both exocrine and endocrine tissues, whereas larger molecules such as 10 kDa dextran diffused more rapidly out of the latter, suggesting that islets only perceive 'flashes' of circulating molecules and that passive retention by the tissue is very limited. Such findings might partly explain why beta cells *in vivo* are less proliferative than some cell types in other tissues, where the microenvironment better supports the retention and build-up of mitotic factors [39].

Gestation is characterized by beta cell expansion and modifications in beta cell activity and hormonal balance [11]. HFD-feeding induces a similar adaptive response, albeit in a pregnancy hormone-independent context. Under both conditions, extravasation was unexpectedly reduced, suggesting that beta cells experience delayed exposure to circulating molecules during heightened insulin demand. This reduced extravasation likely results from a decrease in transfer rate of molecules across the vascular membrane, rather than active removal from the tissue, i.e. through lymphatic drainage, since lymphatics are rarely associated with islets [40]. Moreover, molecule fluorescence profile was modeled in the ascending phase, where extravasation rate has more pronounced effects than clearance. However, a contribution of the latter to the measures detailed here cannot be ruled out. This notwithstanding, alterations to molecule exposure might provide a mechanism to downregulate insulin signaling during gestation, helping to maintain the hyperglycemia required to support the energy requirements of fetal growth, and may partly explain the impaired insulin secretion detected in mice *in vivo* one week after commencing HFD [13–15], despite improved beta cell function in isolated islets [41]. Importantly, this demonstrates that molecule diffusion is a dynamic process modulated by physiological state.

Increased islet vessel volume during gestation may be explained by both marked islet endothelial proliferation [30] and vessel dilation, as supported by the observed increase in the perimeters of a subset of islet vessels at G14.5. By contrast, changes in the islet vasculature during long-term HFD treatment depend solely on dilation, and not angiogenesis [19], supporting a role for divergent mechanisms in controlling adaptation to metabolic demand. We did not observe an increase in islet vessel perimeter after 2 weeks of HFD feeding, suggesting that dilation is triggered during later stages of treatment [19]. Although it was previously reported that fenestrae density may contribute to the acute regulation of molecule

entry into tissues due to their rapid turnover/appearance [3], no change in mean fenestrae diameter or density was detected. We cannot, however, exclude a role for alterations in the composition of fenestrae diaphragms, which act as size-selective molecular sieves involved in the regulation of basal permeability [42, 43].

It has been shown that the perivascular space can provide a niche for cell proliferation [44]. Therefore, it is plausible that beta cell proliferation may directly affect islet capillary properties to favor this process. We therefore tested whether inhibition of beta cell proliferation during gestation, through suppression of serotonin synthesis [31], was able to modify vascular permeability in islets. We found that, besides proliferation, the structural changes occurring at G14.5 were unaffected, and permeability in islets was decreased compared to virgin mice fed with TRP- diet, possibly through similar mechanisms to gestation under normal feeding. Therefore, neither beta cell proliferation nor increased serotonin levels appear to be instructive for decreased molecule exposure during gestation, despite the reported vasoactive properties of the latter monoamine [45]. Alternative mechanisms may include prolactin/placental lactogen, whose circulating levels peak during gestation. Both these peptides may regulate vascular plasticity/permeability through signaling directly to endothelial cells [46, 47], as well as increasing vascular endothelial growth factor production [30].

The modifications to vascular permeability measured using fluorescent-dextran *in vivo* may not be relevant for biologically-active molecules. Indeed, it could be argued that the natural affinity of islets for their substrate may maintain molecule binding/uptake, even in the face of altered permeability during metabolic demand. Suggesting that this is not the case, 2-NBDG uptake rate decreased in islets of gestating animals, despite the reported increase in

GLUT2 expression by G15 [48]. Likewise, 2-NBDG uptake rate was decreased following short-term high fat-feeding, probably reflecting changes in membrane-trafficking of GLUT2 [49]. Although changes in blood flow velocity, generally associated with alterations to capillary pressure [50], may affect 2-NBDG uptake rates, we were unable to detect any differences in red blood cell velocity in virgin, G14.5 and HFD (2 week)-fed animals. While the effects of acutely increased metabolic demand on vascular parameters in awake mice remain unknown, and an effect of anaesthetic and/or blood pressure on tissue perfusion cannot be completely excluded, this demonstrates that the delayed uptake of 2-NBDG is unlikely a consequence of reduced islet blood flow. Thus, the data together suggest that vascular permeability likely contributes to islet (patho)physiology by modifying the exposure of beta cells to bioactive substances.

In summary, we show that beta cells *in vivo* are exposed to peaks of circulating molecule, and that islet vessel permeability and molecule diffusion are dynamic processes, which can be influenced by physiological state. Together with well-characterized molecular and cellular mechanisms, the islet vasculature may thus be targeted by T2D insults to precipitate insulin secretory failure.

ACKNOWLEDGMENTS

The authors declare no conflict of interest. Dr. Marie Schaeffer is the guarantor of this work and, as such, had full access to all the data in the study and takes responsibility for the integrity of the data and the accuracy of the data analysis. DJH, PM and MS designed experiments; AM, DJH, AG, GEC, and MS performed experiments; AM, DJH, PF, FM and MS analyzed data; CJP, ICR and PLT produced transgenic mice; DJH, PM and MS wrote the manuscript. The authors would like to thank C. Lafont and Dr. M. Desarménien, Institute of Functional Genomics, Montpellier, for technical assistance with surgery, Dr. C. Cazevieille, Centre Régional d'Imagerie Cellulaire, Montpellier, for assistance with the electron microscope, Dr. M. Strom, National Institute for Medical Research, London, for help with transgenic mouse model production, Dr. X. Bonnefont, Institute of Functional Genomics, Montpellier, for useful comments on the manuscript, and all the animal facility staff at the Institute of Functional Genomics. Authors were supported by grants from the Agence Nationale de la Recherche (ANR BETA-DYN JCJC13 to MS), INSERM, CNRS, University of Montpellier, National Biophotonics and Imaging Platform of Ireland (NBIPI), IBiSA, Diabetes UK (RD Lawrence Fellowship; 12/0004431 to DJH), Medical Research Council (MR/N00275X/1 to DJH), European Foundation for the Study of Diabetes (EFSD/Novo Nordisk Rising Star Fellowship to DJH), and Région Languedoc-Roussillon (IPAM).

REFERENCES

1. Steiner DJ, Kim A, Miller K, Hara M (2010) Pancreatic islet plasticity: interspecies comparison of islet architecture and composition. Islets 2:135–145.

2. Hara M, Dizon RF, Glick BS, et al. (2006) Imaging pancreatic beta-cells in the intact pancreas. Am J Physiol Endocrinol Metab 290:E1041–7. doi: 10.1152/ajpendo.00365.2005

3. Henderson JR, Moss MC (1985) A morphometric study of the endocrine and exocrine capillaries of the pancreas. Q J Exp Physiol 70:347–356.

4. Jansson L, Hellerstrom C (1983) Stimulation by glucose of the blood flow to the pancreatic islets of the rat. Diabetologia 25:45–50.

5. Schaeffer M, Hodson DJ, Lafont C, Mollard P (2011) Endocrine cells and blood vessels work in tandem to generate hormone pulses. J Mol Endocrinol 47:R59–66. doi: 10.1530/JME-11-0035

6. Campbell JE, Drucker DJ (2013) Pharmacology, physiology, and mechanisms of incretin hormone action. Cell Metab 17:819–837. doi: 10.1016/j.cmet.2013.04.008

7. Brelje TC, Bhagroo N V, Stout LE, Sorenson RL (2008) Beneficial effects of lipids and prolactin on insulin secretion and beta-cell proliferation: a role for lipids in the adaptation of islets to pregnancy. J Endocrinol 197:265–276. doi: 10.1677/JOE-07-0657

8. Huang C, Snider F, Cross JC (2009) Prolactin receptor is required for normal glucose homeostasis and modulation of beta-cell mass during pregnancy. Endocrinology 150:1618–1626. doi: 10.1210/en.2008-1003

9. Sachdeva MM, Stoffers DA (2009) Minireview: Meeting the demand for insulin: molecular mechanisms of adaptive postnatal beta-cell mass expansion. Mol Endocrinol 23:747–758. doi: 10.1210/me.2008-0400

10. Nolan CJ, Damm P, Prentki M (2011) Type 2 diabetes across generations: from pathophysiology to prevention and management. Lancet 378:169–181. doi: 10.1016/S0140-6736(11)60614-4

11. Sorenson RL, Brelje TC (1997) Adaptation of islets of Langerhans to pregnancy: beta-cell growth, enhanced insulin secretion and the role of lactogenic hormones. Horm Metab Res 29:301–307. doi: 10.1055/s-2007-979040

12. Rieck S, White P, Schug J, et al. (2009) The transcriptional response of the islet to pregnancy in mice. Mol Endocrinol 23:1702–1712. doi: 10.1210/me.2009-0144

13. Stamateris RE, Sharma RB, Hollern DA, Alonso LC (2013) Adaptive beta-cell proliferation increases early in high-fat feeding in mice, concurrent with metabolic changes, with induction of islet cyclin D2 expression. Am J Physiol Endocrinol Metab 305:E149–59. doi: 10.1152/ajpendo.00040.2013

14. Mosser RE, Maulis MF, Moullé VS, et al. (2015) High Fat Diet-Induced Beta Cell Proliferation Occurs Prior to Insulin Resistance in C57Bl/6J Male Mice. Am J Physiol - Endocrinol Metab ajpendo.00460.2014. doi: 10.1152/ajpendo.00460.2014

15. Winzell MS, Ahren B (2004) The high-fat diet-fed mouse: a model for studying mechanisms and treatment of impaired glucose tolerance and type 2 diabetes. Diabetes 53 Suppl 3:S215–9.

16. Carlsson P-O, Olsson R, Källskog O, et al. (2002) Glucose-induced islet blood flow increase in rats: interaction between nervous and metabolic mediators. Am J Physiol Endocrinol Metab 283:E457–E464. doi: 10.1152/ajpendo.00044.2002

17. Carlsson PO, Andersson A, Jansson L (1998) Influence of age, hyperglycemia, leptin, and NPY on islet blood flow in obese-hyperglycemic mice. Am J Physiol 275:E594–E601.

18. Nyman LR, Ford E, Powers AC, Piston DW (2010) Glucose-dependent blood flow dynamics in murine pancreatic islets in vivo. Am J Physiol Endocrinol Metab 298:E807–E814. doi: 10.1152/ajpendo.00715.2009

19. Dai C, Brissova M, Reinert RB, et al. (2013) Pancreatic islet vasculature adapts to insulin resistance through dilation and not angiogenesis. Diabetes 62:4144–4153. doi: 10.2337/db12-1657

20. Svensson AM, Bodin B, Andersson A, Jansson L (2004) Pancreatic islet blood flow during pregnancy in the rat: An increased islet mass is associated with decreased islet blood flow. J Endocrinol 180:409–415. doi: 10.1677/joe.0.1800409

21. Hashimoto S, Kubota N, Sato H, et al. (2015) Insulin Receptor Substrate-2 (Irs2) in Endothelial Cells Plays a Crucial Role in Insulin Secretion. Diabetes 64:876–886. doi: 10.2337/db14-0432

22. He Z, Fernandez-Fuente M, Strom M, et al. (2011) Continuous on-line monitoring of secretion from rodent pituitary endocrine cells using fluorescent protein surrogate markers. J Neuroendocr 23:197–207. doi: 10.1111/j.1365-2826.2010.02104.x

23. Bates P, Young JA, Varmus HE (1993) A receptor for subgroup A Rous sarcoma virus is related to the low density lipoprotein receptor. Cell 74:1043–1051.

24. Lemaire K, Ravier MA, Schraenen A, et al. (2009) Insulin crystallization depends on zinc transporter ZnT8 expression, but is not required for normal glucose homeostasis in mice. Proc Natl Acad Sci U S A 106:14872–14877. doi: 10.1073/pnas.0906587106

25. Lafont C, Desarmenien MG, Cassou M, et al. (2010) Cellular in vivo imaging reveals coordinated regulation of pituitary microcirculation and GH cell network function. Proc Natl Acad Sci U S A 107:4465–4470. doi: 10.1073/pnas.0902599107

26. Schaeffer M, Langlet F, Lafont C, et al. (2013) Rapid sensing of circulating ghrelin by hypothalamic appetite-modifying neurons. Proc Natl Acad Sci U S A 110:1512–1517. doi: 10.1073/pnas.1212137110

27. Kulandavelu S, Qu D, Adamson SL (2006) Cardiovascular function in mice during normal pregnancy and in the absence of endothelial NO synthase. Hypertension 47:1175–1182. doi: 10.1161/01.HYP.0000218440.71846.db

28. Sun G, Tarasov AI, McGinty JA, et al. (2010) LKB1 deletion with the RIP2.Cre transgene modifies pancreatic beta-cell morphology and enhances insulin secretion in vivo. Am J Physiol Endocrinol Metab 298:E1261–73. doi: 10.1152/ajpendo.00100.2010

29. Guillou A, Romanò N, Bonnefont X, et al. (2011) Modulation of the tyrosine kinase receptor ret/glial cell-derived neurotrophic factor (GDNF) signaling: A new player in reproduction induced anterior pituitary plasticity? Endocrinology 152:515–525. doi: 10.1210/en.2010-0673

30. Johansson M, Mattsson G, Andersson A, et al. (2006) Islet endothelial cells and pancreatic beta-cell proliferation: studies in vitro and during pregnancy in adult rats. Endocrinology 147:2315–2324. doi: 10.1210/en.2005-0997

31. Kim H, Toyofuku Y, Lynn FC, et al. (2010) Serotonin regulates pancreatic beta cell mass during pregnancy. Nat Med 16:804–808. doi: 10.1038/nm.2173

32. Saha JK, Xia J, Grondin JM, et al. (2005) Acute hyperglycemia induced by ketamine/xylazine anesthesia in rats: mechanisms and implications for preclinical models. Exp Biol Med (Maywood) 230:777–784. doi: 230/10/777 [pii]

33. Forbes JM, Cooper ME (2013) Mechanisms of diabetic complications. Physiol Rev 93:137–88. doi: 10.1152/physrev.00045.2011

34. Richards OC, Raines SM, Attie AD (2010) The role of blood vessels, endothelial cells, and vascular pericytes in insulin secretion and peripheral insulin action. Endocr Rev 31:343–363. doi: 10.1210/er.2009-0035

35. Reinbothe TM, Safi F, Axelsson AS, et al. (2014) Optogenetic control of insulin secretion in intact pancreatic islets with β-cell-specific expression of Channelrhodopsin-2. Islets. doi: 10.4161/isl.28095

36. Tarasov AI, Semplici F, Ravier MA, et al. (2012) The mitochondrial Ca2+ uniporter MCU is essential for glucose-induced atp increases in pancreatic ??-cells. PLoS One. doi: 10.1371/journal.pone.0039722

37. Kokovay E, Goderie S, Wang Y, et al. (2010) Adult SVZ lineage cells home to and leave the vascular niche via differential responses to SDF1/CXCR4 signaling. Cell Stem Cell 7:163–173. doi: 10.1016/j.stem.2010.05.019

38. Charles N, Holland EC (2010) The perivascular niche microenvironment in brain tumor progression. Cell Cycle 9:3012–3021. doi: 10.4161/cc.9.15.12710

39. Morrison SJ, Scadden DT (2014) The bone marrow niche for haematopoietic stem cells. Nature 505:327–34. doi: 10.1038/nature12984

40. O'Morchoe CCC (1997) Lymphatic system of the pancreas. Microsc Res Tech 37:456–477. doi: 10.1002/(SICI)1097-0029(19970601)37:5/6<456::AID-JEMT9>3.0.CO;2-B

41. Collins SC, Hoppa MB, Walker JN, et al. (2010) Progression of diet-induced diabetes in C57BL6J mice involves functional dissociation of Ca2(+) channels from secretory vesicles. Diabetes 59:1192–1201. doi: 10.2337/db09-0791

42. Stan R V., Tse D, Deharvengt SJ, et al. (2012) The Diaphragms of Fenestrated Endothelia: Gatekeepers of Vascular Permeability and Blood Composition. Dev Cell 23:1203–1218. doi: 10.1016/j.devcel.2012.11.003

43. Deharvengt SJ, Tse D, Sideleva O, et al. (2012) PV1 down-regulation via shRNA inhibits the growth of pancreatic adenocarcinoma xenografts. J Cell Mol Med 16:2690–2700. doi: 10.1111/j.1582-4934.2012.01587.x

44. Eberhard D, Kragl M, Lammert E (2010) "Giving and taking": endothelial and beta-cells in the islets of Langerhans. Trends Endocrinol Metab 21:457–463. doi: 10.1016/j.tem.2010.03.003

45. Colditz IG (1991) The induction of plasma leakage in skin by histamine, bradykinin, activated complement, platelet-activating factor and serotonin. Immunol Cell Biol 69 (Pt 3):215–219. doi: 10.1038/icb.1991.31

46. Merkle CJ, Schuler LA, Schaeffer RC, et al. (2000) Structural and functional effects of high prolactin levels on injured endothelial cells: evidence for an endothelial prolactin receptor. Endocrine 13:37–46. doi: 10.1385/ENDO:13:1:37

47. Kolonin MG, Sun J, Do KA, et al. (2006) Synchronous selection of homing peptides for multiple tissues by in vivo phage display. Faseb J 20:979–981. doi: 10.1096/fj.05-5186fje

48. Weinhaus AJ, Stout LE, Sorenson RL (1996) Glucokinase, hexokinase, glucose transporter 2, and glucose metabolism in islets during pregnancy and prolactin-treated islets in vitro: Mechanisms for long term up-regulation of islets. Endocrinology 137:1640–1649. doi: 10.1210/en.137.5.1640

49. Reimer MK, Ahrén B (2002) Altered β-cell distribution of pdx-1 and GLUT-2 after a short-term challenge with a high-fat diet in C57BL/6J mice. Diabetes. doi: 10.2337/diabetes.51.2007.S138

50. Carlsson PO, Jansson L, Andersson A, Kallskog O (1998) Capillary blood pressure in syngeneic rat islets transplanted under the renal capsule is similar to that of the implantation organ . Diabetes 47:1586–1593.

FIGURES LEGENDS

Figure 1. *In vivo* molecule diffusion and extravasation in islets. V: Virgin. A-B) Schematic representation of the imaging setup: side view (A), ventral view (B). 1: tracheotomy, 2: jugular catheter, 3: heated saline perfusion, 4: temperature control. C) Fluorescence variation at three time points after i.v. injection of 4 kDa fluorescent dextran, in the exocrine tissue (top), and in islets (bottom; dashed circle) (Scale: 100 μm). Tmax corresponds to time at which fluorescence intensity is maximum in the vessels. Green: FITC. Fluorescence variations were measured in regions of interest (blue and red dots). See also Movie S1. D) Fluorescence intensity profiles over time post-injection of 4 kDa fluorescent dextran (AU) in vessels (red lines) and parenchyma (blue lines) of the endocrine (left) and exocrine (right) tissues. Lines correspond to times points at which pictures in (C) were taken. E) Molecule extravasation rate as a function of MW (n = 4-8 mice per condition; 1-2 movies/mouse). F) Fluorescence decrease rate measured in tissue parenchyma, as a function of MW (n = 4-8 mice per condition; 1-2 movies/mouse, one-way ANOVA). Values represent mean ± SEM.

Figure 2. **Islet and beta cell modifications at G14.5 of gestation.** A) Representative confocal images of islets in virgin animals and at G14.5 (scale bar: 50 µm, Z-projection of 16 µm stacks). B) Islet size is increased at G14.5 (n = 6 animals per condition; P<0.0005 Mann-Whitney test). C) Beta cells are hypertrophic at G14.5 (n = 6 animals per condition; P<0.001 Mann-Whitney test). D-E) Basal insulin level is increased (n = 4-5 mice per condition, P<0.05 Mann-Whitney test), while glucose-stimulated insulin secretion is unchanged at G14.5, as assessed by measurement of the increase in plasma insulin concentration post-glucose injection (3 g/kg) (e) (n = 4-5 mice per condition, two-way ANOVA). F) Representative confocal images of Ki67 labeling in virgin animals and at G14.5 (same islets as in A) (scale bar: 50 µm, Z-projection of 16 µm stacks). G) Proliferation is increased at G14.5 (n = 6 animals per condition; P<0.001 Mann-Whitney test). H-I) IPGTT (2g/kg) in virgin and at G14.5 (H), and area under the curve (AUC) analysis (I) shows glucose intolerance at G14.5 (n = 6-8 animals per condition, P<0.01 Mann-Whitney test). Values represent mean ± SEM.

Figure 3. **Glucose metabolism and beta cell proliferation are altered by 2 weeks of high fat diet.** SD: standard diet, HFD: high fat diet. A) Body weight increase was larger in mice fed HFD (n = 18 mice per condition; two-way ANOVA). B) Randomly fed blood glucose levels were higher in HFD fed mice (n = 30 mice per condition; two-way ANOVA). C-D) IPGTT (2g/kg) in SD and HFD fed animals (C), and area under the curve (AUC) analysis (D) shows glucose intolerance (n = 11 animals per condition, P<0.01 Mann-Whitney test). E) Glucose-stimulated insulin secretion (3 g/kg) is not significantly decreased by 2 weeks HFD (n = 5 mice per condition, two-way ANOVA). F) Representative confocal images of islets in animals fed standard chow (SD) or HFD for 2 weeks (scale bar: 100 µm, Z-projection of 16 µm stacks). G) Islet size is not modified (n = 6 animals, 40-80 islets per condition; one-way ANOVA). H) Beta cells are hypertrophic at HFD 2 weeks (n = 6 animals per condition;

P<0.001 Mann-Whitney test). I) Representative confocal images of Ki67 labeling in SD or HFD fed animals (scale bar: 100 μm, Z-projection of 16 μm stacks). J) Proliferation is increased following 2 weeks HFD feeding (n = 6 animals per condition; one-way ANOVA). Values represent mean ± SEM.

Figure 4. Modification of molecule diffusion in islets during metabolic demand. V: Virgin. HFD2w: High-fat-diet 2 weeks. A) Fluorescence variation in an islet (dashed circle) at three time points after i.v. injection of 4 kDa dextran at G14.5 of gestation (see also Movie S2) (Scale: 100 μm). Tmax corresponds to time at which fluorescence intensity is maximum in the vessels. Green: FITC. Fluorescence variations were measured in regions of interest (blue dots). Comparable images in virgin animals can be found in Fig. 1C. B) Molecule extravasation rate as a function of MW (n = 4-8 mice per condition; 1-2 movies/mouse) at G14.5. C) Fluorescence decrease rate in tissue parenchyma, as a function of MW at G14.5 (n = 4-9 mice per condition; 1-2 movies/mouse; one-way ANOVA). D) Fluorescence variation in an islet (dashed circle) at three time points after i.v. injection of 4 kDa dextran following 2 weeks of HFD (see also Movie S3) (Scale: 100μm). Green: FITC. Fluorescence variations were measured in regions of interest (blue dots). E) Molecule extravasation rate as a function of molecular weight (n = 4-8 mice per condition; 1-2 movies/mouse) following 2 weeks of HFD. F) Fluorescence decrease rate in tissue parenchyma as a function of molecular weight (n = 4-9 mice per condition; 1-2 movies/mouse; one-way ANOVA) following 2 weeks of HFD. Values represent mean ± SEM.

Figure 5. **Alterations to vessels in response to gestation and HFD.** SD: standard diet, HFD: high fat diet. V: virgin. Values represent mean ± SEM. A-B) Representative confocal images

of islet vasculature in virgin and gestating (G14.5) animals (A, left), and SD and HFD fed animals (B, left) (scale: 10 μm). Z-projections of 26 (A) or 15 (B) μm stacks. Percentage of islet volume occupied by vessels (A-B, right panels) (n = 6 mice, 3-10 islets per mouse; $P<0.01$ (A) and $P = 0.19$ (B); Student t-test). C) Representative transmission electron microscopy (TEM) images of islet vessels from virgin, G14.5 and HFD 2 weeks animals (scale: 10 μm). D) Islet vessels lumen perimeter is increased at G14.5 compared to virgin animals (n = 2 mice, 14-17 vessels per condition, $P<0.01$, Student t-test). E) Islet vessel lumen perimeter is unchanged in HFD 2 weeks compared to standard fed animals (n = 2 mice, 17-25 vessels per condition, $P=0.11$, Student t-test). F) Representative TEM images of islet vessels in virgin and G14.5 animals (scale: 1 μm). Boxed areas (left) are enlarged (right). Arrows indicate fenestrations. G) Density of fenestrations per μm of endothelium shows no variation between virgin and G14.5 (n = 2 mice per condition, 20-48 μm endothelium; $P=0.2854$ Student t-test). H) Density of fenestrations is unchanged by HFD 2 weeks (n = 2 mice per condition, 25-48 μm endothelium; $P = 0.8372$ Student t-test). I) Representative TEM images of islet vessels cut en-face (scale bar: 1 μm). Boxed areas are enlarged (right). Arrows indicate fenestrations. J) Fenestrae diameter measurement shows no variation between virgin and G14.5 (n = 2 mice per condition, 100 fenestrae; $P = 0.055$ Student t-test). K) Fenestrae diameter measurement shows no variation after 2 weeks HFD (n = 2 mice per condition, 55-115 fenestrae; $P = 0.072$ Student t-test).

Figure 6. Inhibition of beta cell proliferation during gestation is not associated with altered permeability. V: virgin. TRP: tryptophan. A) Body weight of animals fed TRP+/- diet 6 days (n = 9-14 mice per condition; one-way ANOVA). B-C) IPGTT (2g/kg) (B) and analysis of AUC (C) (n = 6-7 mice per condition; one-way ANOVA). D) Representative confocal images of islets in virgin or G14.5 animals fed TRP- diet (scale: 100 μm, Z-

projection of 11 µm stacks). E) Quantification of islet volume (n = 6 mice per condition; one-way ANOVA). F) Representative labeling by Ki67 of nuclei in islets in virgin or G14.5 animals fed TRP- diet. G) Quantification of Ki67+ nuclei in islets (n = 6 mice per condition; one-way ANOVA). H) Fluorescence variation in islets at two time points post i.v. injection of 4 kDa dextran (virgin TRP-; top, G14.5 TRP-; bottom) (Scale: 100 µm). Tmax corresponds to time at which fluorescence intensity is maximum in the vessels. Green: FITC. Fluorescence variations were measured in regions of interest (blue dots). See also Movie S4. I) Molecule extravasation rate as a function of MW (n = 4-8 mice per condition; 1-2 movies/mouse; two-way ANOVA). Values represent mean ± SEM.

Figure 7. Measure of 2-NBDG uptake rate *in vivo*. A) Fluorescence variation in islets at three time points post i.m. injection of 2-NBDG (10 mg/kg) (virgin; top, G14.5; middle, HFD 2 weeks; bottom) (Scale: 100 µm, Z-projection of 120 µm). Islets (circled) are easily identified by labeling of vessels with rhodamine-dextran (red). Green: 2-NBDG. See also Movie S5. B) Measurement of 2-NBDG fluorescence in islets over time post injection i.m.: normalized fluorescence profiles fitted with sigmoidal curves (left panel), and first derivatives of fitted sigmoidal curves (right panel) (n = 4-6 mice per condition, 1-2 islets/mouse; Mann-Whitney test of inflexion points (left) and Vmax (right)). NF: normalized fluorescence, T: time. Values represent mean ± SEM. C) As for A), but fluorescence variation in islets at three time points post i.v. injection of 2-NBDG (5 mg/kg) (virgin; top, G14.5; middle, HFD 2 weeks; bottom) (Scale: 100 µm, Z-projection of 120 µm). See also Movie S6. D) Measurement of 2-NBDG fluorescence in islets over time post injection i.v.: normalized fluorescence profiles fitted with one-phase association curves (n = 4-5 mice per condition, 1-2 islets/mouse; Mann-Whitney test of inflexion points). Values represent mean ± SEM.

Figure 8. ***In vivo*** **red blood cells velocity in islets is comparable between G14.5, 2 weeks HFD-fed and virgin animals.** A) Still images extracted from movies of pancreatic blood flow in a virgin mouse acquired *in vivo*. See also Movie S7. Islet is circled. Bars indicate vessels selected for analysis. Grey: 150 kDa FITC-dextran. Image size: 274x274 μm. B) Red blood cell (RBC) velocity measured in exocrine tissue and islets in virgin, G14.5, and 2 week HFD-fed animals. Each dot represents an individual vessel (n = 5-6 animals per condition, one-way ANOVA). Data is represented as mean ± SEM. C) Blood glucose levels following ketamine/xylaxine anesthesia (n = 5-6 animals per condition, no significant difference, two-way ANOVA). Data is represented as mean ± SEM.

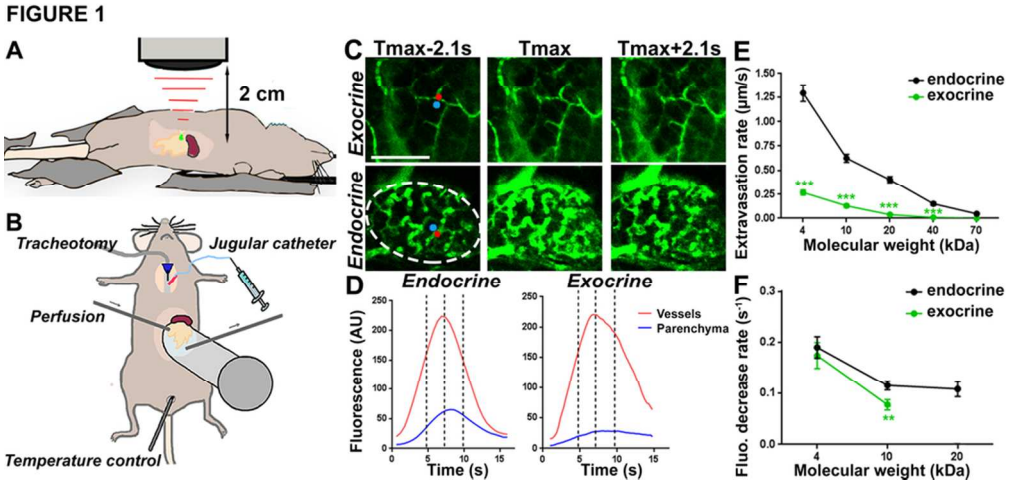

Figure 1. In vivo molecule diffusion and extravasation in islets. V: Virgin. A-B) Schematic representation of the imaging setup: side view (A), ventral view (B). 1: tracheotomy, 2: jugular catheter, 3: heated saline perfusion, 4: temperature control. C) Fluorescence variation at three time points after i.v. injection of 4 kDa fluorescent dextran, in the exocrine tissue (top), and in islets (bottom; dashed circle) (Scale: 100 µm). Tmax corresponds to time at which fluorescence intensity is maximum in the vessels. Green: FITC. Fluorescence variations were measured in regions of interest (blue and red dots). See also Movie S1. D) Fluorescence intensity profiles over time post-injection of 4 kDa fluorescent dextran (AU) in vessels (red lines) and parenchyma (blue lines) of the endocrine (left) and exocrine (right) tissues. Lines correspond to times points at which pictures in (C) were taken. E) Molecule extravasation rate as a function of MW (n = 4-8 mice per condition; 1-2 movies/mouse). F) Fluorescence decrease rate measured in tissue parenchyma, as a function of MW (n = 4-8 mice per condition; 1-2 movies/mouse, one-way ANOVA). Values represent mean ± SEM.

88x43mm (300 x 300 DPI)

FIGURE 2

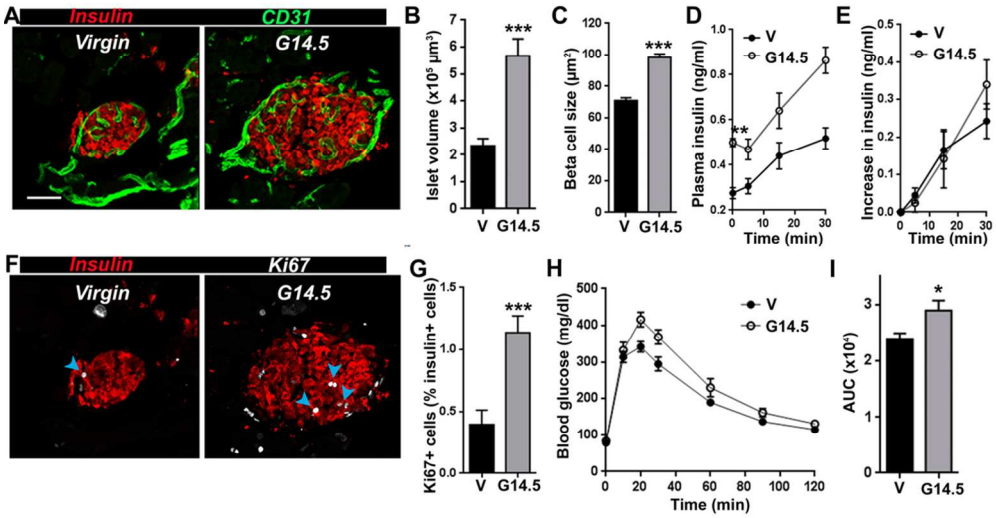

Figure 2. Islet and beta cell modifications at G14.5 of gestation. A) Representative confocal images of islets in virgin animals and at G14.5 (scale bar: 50 µm, Z-projection of 16 µm stacks). B) Islet size is increased at G14.5 (n = 6 animals per condition; P<0.0005 Mann-Whitney test). C) Beta cells are hypertrophic at G14.5 (n = 6 animals per condition; P<0.001 Mann-Whitney test). D-E) Basal insulin level is increased (n = 4-5 mice per condition, P<0.05 Mann-Whitney test), while glucose-stimulated insulin secretion is unchanged at G14.5, as assessed by measurement of the increase in plasma insulin concentration post-glucose injection (3 g/kg) (e) (n = 4-5 mice per condition, two-way ANOVA). F) Representative confocal images of Ki67 labeling in virgin animals and at G14.5 (same islets as in A) (scale bar: 50 µm, Z-projection of 16 µm stacks). G) Proliferation is increased at G14.5 (n = 6 animals per condition; P<0.001 Mann-Whitney test). H-I) IPGTT (2g/kg) in virgin and at G14.5 (H), and area under the curve (AUC) analysis (I) shows glucose intolerance at G14.5 (n = 6-8 animals per condition, P<0.01 Mann-Whitney test). Values represent mean ± SEM.

100x56mm (300 x 300 DPI)

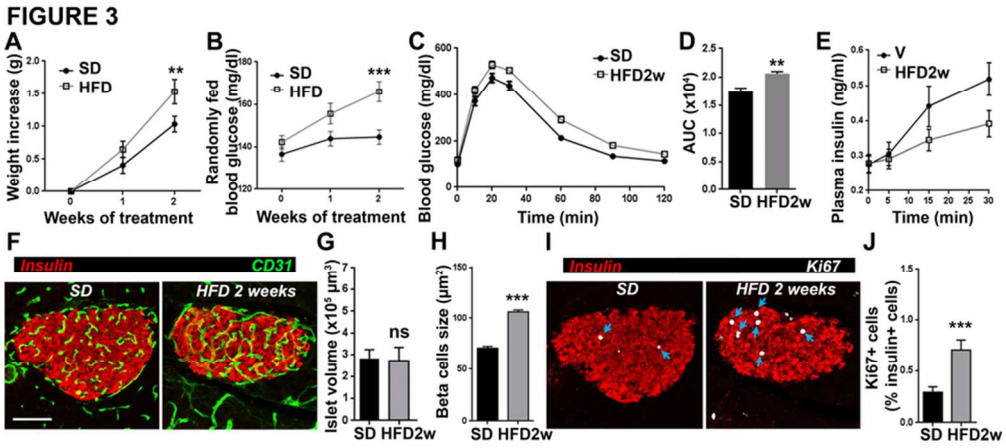

Figure 3. Glucose metabolism and beta cell proliferation are altered by 2 weeks of high fat diet. SD: standard diet, HFD: high fat diet. A) Body weight increase was larger in mice fed HFD (n = 18 mice per condition; two-way ANOVA). B) Randomly fed blood glucose levels were higher in HFD fed mice (n = 30 mice per condition; two-way ANOVA). C-D) IPGTT (2g/kg) in SD and HFD fed animals (C), and area under the curve (AUC) analysis (D) shows glucose intolerance (n = 11 animals per condition, $P<0.01$ Mann-Whitney test). E) Glucose-stimulated insulin secretion (3 g/kg) is not significantly decreased by 2 weeks HFD (n = 5 mice per condition, two-way ANOVA). F) Representative confocal images of islets in animals fed standard chow (SD) or HFD for 2 weeks (scale bar: 100 µm, Z-projection of 16 µm stacks). G) Islet size is not modified (n = 6 animals, 40-80 islets per condition; one-way ANOVA). H) Beta cells are hypertrophic at HFD 2 weeks (n = 6 animals per condition; $P<0.001$ Mann-Whitney test). I) Representative confocal images of Ki67 labeling in SD or HFD fed animals (scale bar: 100 µm, Z-projection of 16 µm stacks). J) Proliferation is increased following 2 weeks HFD feeding (n = 6 animals per condition; one-way ANOVA). Values represent mean ± SEM.

81x37mm (300 x 300 DPI)

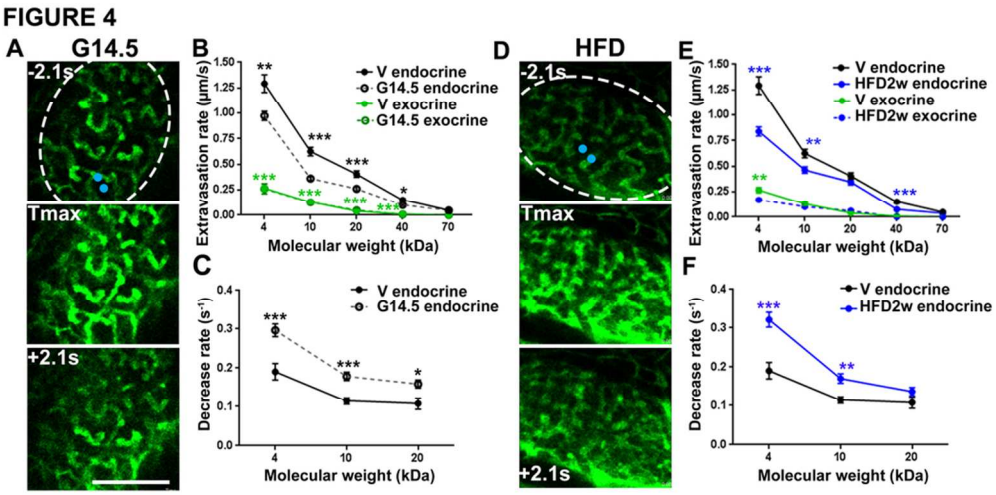

Figure 4. Modification of molecule diffusion in islets during metabolic demand. V: Virgin. HFD2w: High-fat-diet 2 weeks. A) Fluorescence variation in an islet (dashed circle) at three time points after i.v. injection of 4 kDa dextran at G14.5 of gestation (see also Movie S2) (Scale: 100 µm). Tmax corresponds to time at which fluorescence intensity is maximum in the vessels. Green: FITC. Fluorescence variations were measured in regions of interest (blue dots). Comparable images in virgin animals can be found in Fig. 1C. B) Molecule extravasation rate as a function of MW (n = 4-8 mice per condition; 1-2 movies/mouse) at G14.5. C) Fluorescence decrease rate in tissue parenchyma, as a function of MW at G14.5 (n = 4-9 mice per condition; 1-2 movies/mouse; one-way ANOVA). D) Fluorescence variation in an islet (dashed circle) at three time points after i.v. injection of 4 kDa dextran following 2 weeks of HFD (see also Movie S3) (Scale: 100µm). Green: FITC. Fluorescence variations were measured in regions of interest (blue dots). E) Molecule extravasation rate as a function of molecular weight (n = 4-8 mice per condition; 1-2 movies/mouse) following 2 weeks of HFD. F) Fluorescence decrease rate in tissue parenchyma as a function of molecular weight (n = 4-9 mice per condition; 1-2 movies/mouse; one-way ANOVA) following 2 weeks of HFD. Values represent mean ± SEM.
89x44mm (300 x 300 DPI)

FIGURE 5

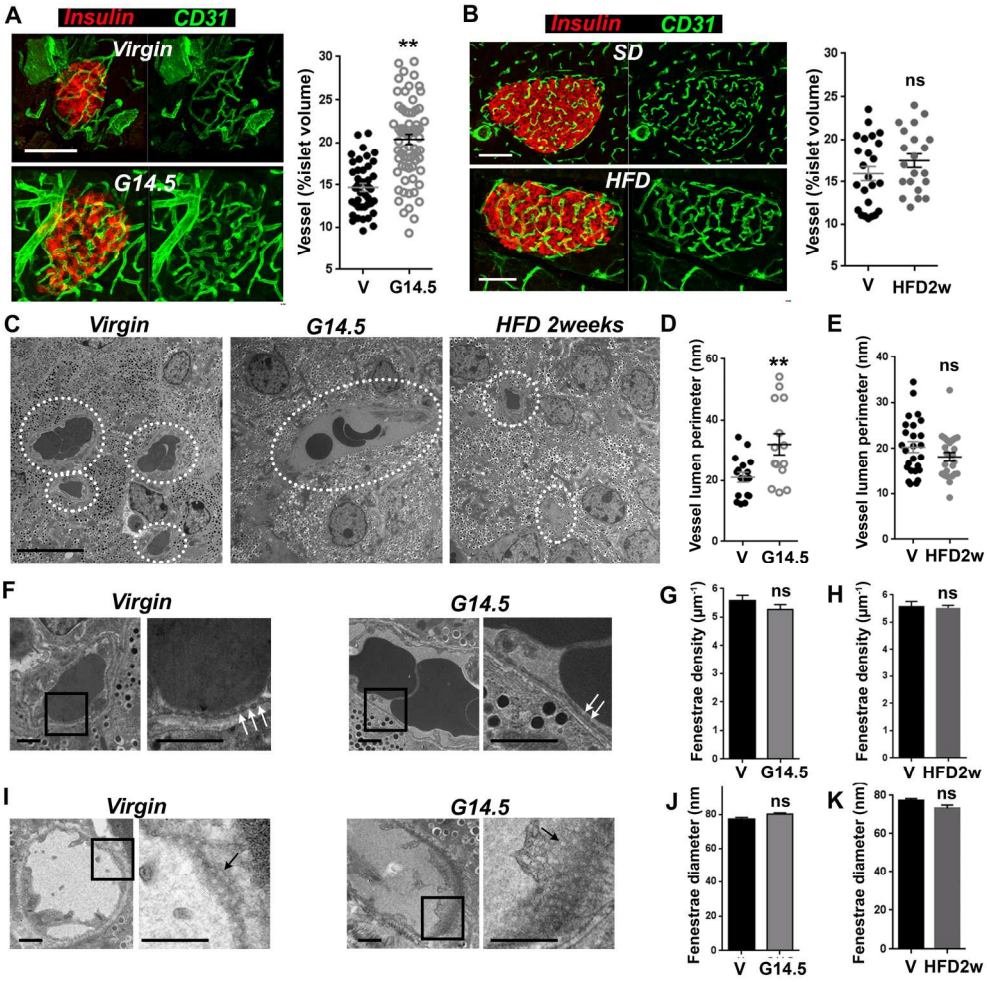

Figure 5. Alterations to vessels in response to gestation and HFD. SD: standard diet, HFD: high fat diet. V: virgin. Values represent mean ± SEM. A-B) Representative confocal images of islet vasculature in virgin and gestating (G14.5) animals (A, left), and SD and HFD fed animals (B, left) (scale: 10 µm). Z-projections of 26 (A) or 15 (B) µm stacks. Percentage of islet volume occupied by vessels (A-B, right panels) (n = 6 mice, 3-10 islets per mouse; P<0.01 (A) and P = 0.19 (B); Student t-test). C) Representative transmission electron microscopy (TEM) images of islet vessels from virgin, G14.5 and HFD 2 weeks animals (scale: 10 µm). D) Islet vessels lumen perimeter is increased at G14.5 compared to virgin animals (n = 2 mice, 14-17 vessels per condition, P<0.01, Student t-test). E) Islet vessel lumen perimeter is unchanged in HFD 2 weeks compared to standard fed animals (n = 2 mice, 17-25 vessels per condition, P=0.11, Student t-test). F) Representative TEM images of islet vessels in virgin and G14.5 animals (scale: 1 µm). Boxed areas (left) are enlarged (right). Arrows indicate fenestrations. G) Density of fenestrations per µm of endothelium shows no variation between virgin and G14.5 (n = 2 mice per condition, 20-48 µm endothelium; P=0.2854 Student t-test). H) Density of fenestrations is unchanged by HFD 2 weeks (n = 2 mice per condition, 25-48 µm endothelium; P = 0.8372 Student t-test). I) Representative TEM images of islet vessels cut en-face (scale bar: 1 µm). Boxed areas are enlarged (right). Arrows indicate fenestrations. J) Fenestrae diameter measurement shows no variation between virgin and G14.5 (n = 2 mice per condition, 100 fenestrae; P = 0.055 Student t-test). K) Fenestrae diameter measurement shows no variation after 2 weeks HFD (n = 2 mice per condition, 55-115 fenestrae; P = 0.072 Student t-test).
186x192mm (300 x 300 DPI)

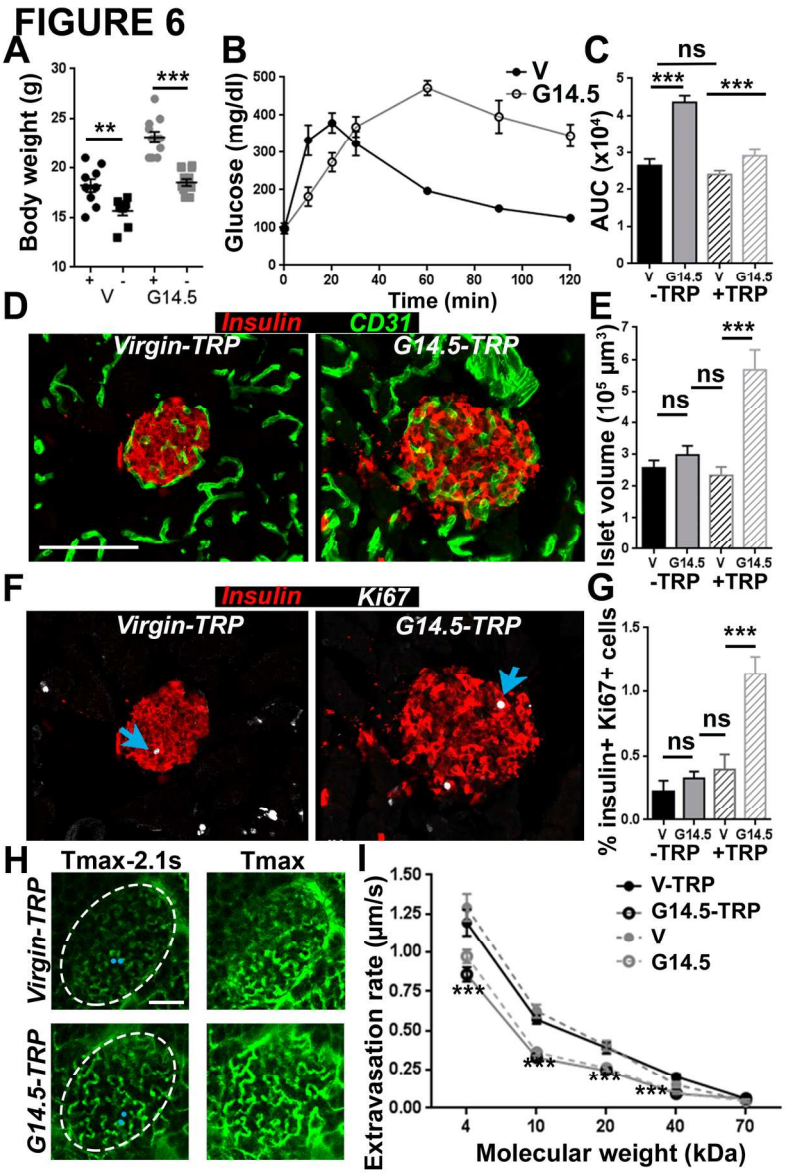

Figure 6. Inhibition of beta cell proliferation during gestation is not associated with altered permeability. V: virgin. TRP: tryptophan. A) Body weight of animals fed TRP+/- diet 6 days (n = 9-14 mice per condition; one-way ANOVA). B-C) IPGTT (2g/kg) (B) and analysis of AUC (C) (n = 6-7 mice per condition; one-way ANOVA). D) Representative confocal images of islets in virgin or G14.5 animals fed TRP- diet (scale: 100 µm, Z-projection of 11 µm stacks). E) Quantification of islet volume (n = 6 mice per condition; one-way ANOVA). F) Representative labeling by Ki67 of nuclei in islets in virgin or G14.5 animals fed TRP- diet. G) Quantification of Ki67+ nuclei in islets (n = 6 mice per condition; one-way ANOVA). H) Fluorescence variation in islets at two time points post i.v. injection of 4 kDa dextran (virgin TRP-; top, G14.5 TRP-; bottom) (Scale: 100 µm). Tmax corresponds to time at which fluorescence intensity is maximum in the vessels. Green: FITC. Fluorescence variations were measured in regions of interest (blue dots). See also Movie S4. I) Molecule extravasation rate as a function of MW (n = 4-8 mice per condition; 1-2 movies/mouse; two-way ANOVA). Values represent mean ± SEM.
136x209mm (300 x 300 DPI)

FIGURE 7

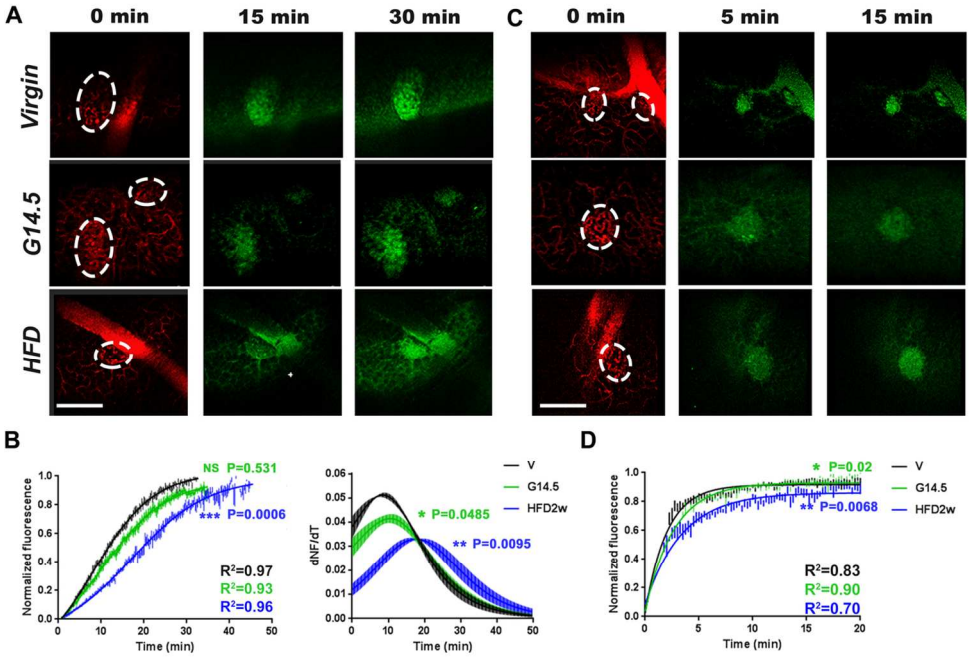

Figure 7. Measure of 2-NBDG uptake rate in vivo. A) Fluorescence variation in islets at three time points post i.m. injection of 2-NBDG (10 mg/kg) (virgin; top, G14.5; middle, HFD 2 weeks; bottom) (Scale: 100 µm, Z-projection of 120 µm). Islets (circled) are easily identified by labeling of vessels with rhodamine-dextran (red). Green: 2-NBDG. See also Movie S5. B) Measurement of 2-NBDG fluorescence in islets over time post injection i.m.: normalized fluorescence profiles fitted with sigmoidal curves (left panel), and first derivatives of fitted sigmoidal curves (right panel) (n = 4-6 mice per condition, 1-2 islets/mouse; Mann-Whitney test of inflexion points (left) and Vmax (right)). NF: normalized fluorescence, T: time. Values represent mean ± SEM. C) As for A), but fluorescence variation in islets at three time points post i.v. injection of 2-NBDG (5 mg/kg) (virgin; top, G14.5; middle, HFD 2 weeks; bottom) (Scale: 100 µm, Z-projection of 120 µm). See also Movie S6. D) Measurement of 2-NBDG fluorescence in islets over time post injection i.v.: normalized fluorescence profiles fitted with one-phase association curves (n = 4-5 mice per condition, 1-2 islets/mouse; Mann-Whitney test of inflexion points). Values represent mean ± SEM.
127x90mm (300 x 300 DPI)

FIGURE 8

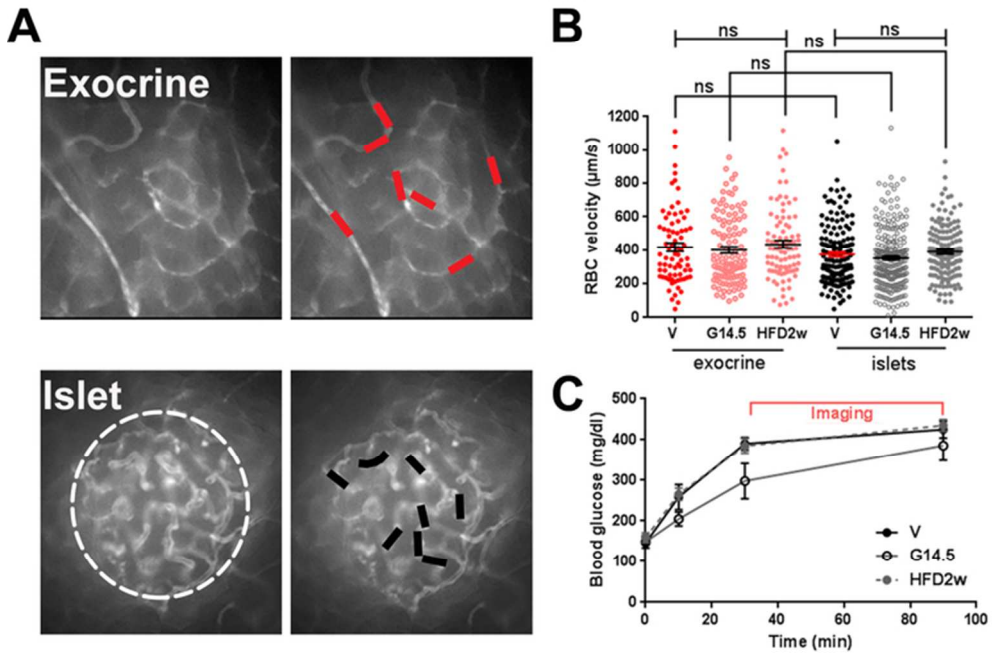

Figure 8. In vivo red blood cells velocity in islets is comparable between G14.5, 2 weeks HFD-fed and virgin animals. A) Still images extracted from movies of pancreatic blood flow in a virgin mouse acquired in vivo. See also Movie S7. Islet is circled. Bars indicate vessels selected for analysis. Grey: 150 kDa FITC-dextran. Image size: 274x274 µm. B) Red blood cell (RBC) velocity measured in exocrine tissue and islets in virgin, G14.5, and 2 week HFD-fed animals. Each dot represents an individual vessel (n = 5-6 animals per condition, one-way ANOVA). Data is represented as mean ± SEM. C) Blood glucose levels following ketamine/xylaxine anesthesia (n = 5-6 animals per condition, no significant difference, two-way ANOVA). Data is represented as mean ± SEM.
64x46mm (300 x 300 DPI)

SUPPLEMENTAL INFORMATION

SUPPLEMENTAL FIGURES

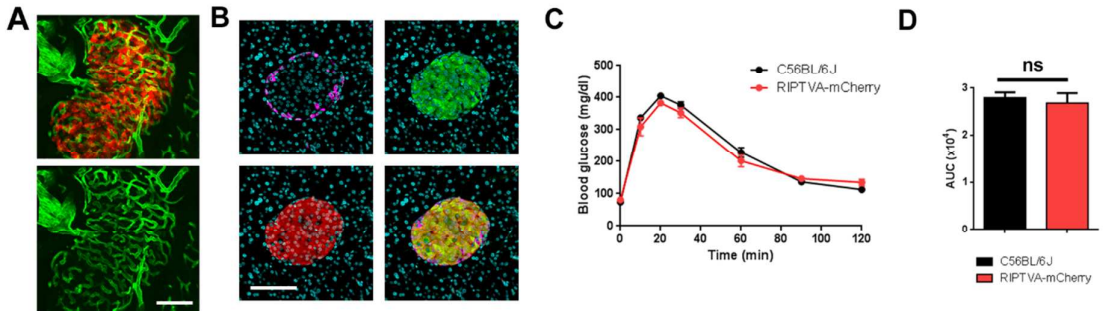

Figure S1

Transgenic RIPTVA-mCherry mice present normal islet morphology and glucose tolerance. A) Representative confocal image of the vasculature in an islet. Z-projection of a 70 µm stack. Red: mCherry, green: vessels (CD31) (scale: 100 µm). B) Reporter mCherry fluorescence is excluded from glucagon-positive cells and co-localizes with insulin-positive cells. Confocal images, Z-projections of 20 µm stacks, purple: glucagon, green: insulin, red: mCherry, blue: dapi (scale: 100 µm). C-D) IPGTT (2g/kg) in virgin C57BL/6J mice and RIPTVA-mCherry mice on a C57BL/6J background (C), and area under the curve (AUC) analysis (D) shows no glucose intolerance in transgenic mice (n = 5 animals per condition, P=0.4127, Mann-Whitney test). Values represent mean ± SEM.

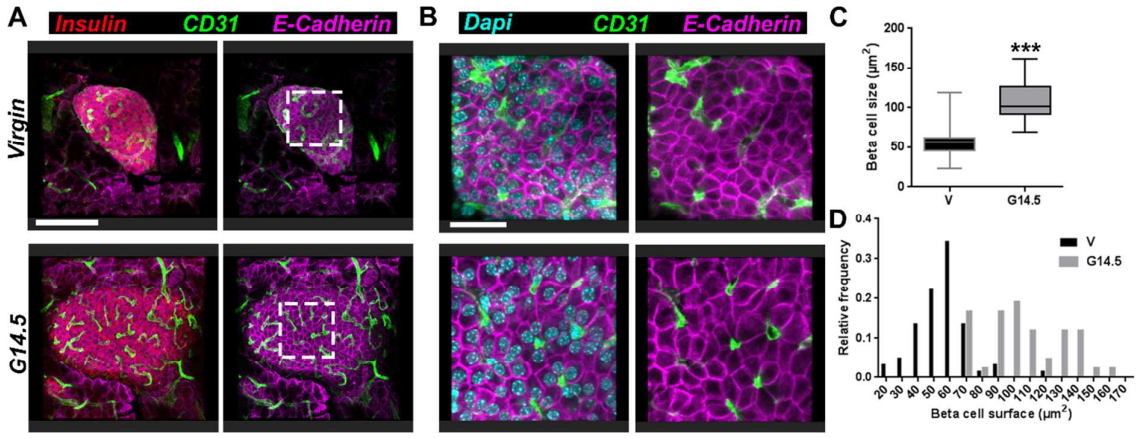

Figure S2

Gestation-induced beta cell hypertrophy. A) Confocal images of islets from virgin and gestating mice (G14.5). Z-projection of a 16 µm stack. Red: insulin, green: vessels (CD31), purple: E-cadherin labeling of membranes (scale: 100 µm). Representative images shown. B) Enlargement of confocal images in (A) (scale: 30 µm). Z-projection of a 3 µm stack. Areas of insulin+ cells presenting a nuclei in cross-section were measured using ImageJ (Dapi staining in blue). C) Mean beta cell size, as measured in the images presented in (B) ($P<0.001$, Mann-Whitney test). Values represent mean with range. D) Frequency distribution (fraction) of beta cell sizes measured in the images in (B).

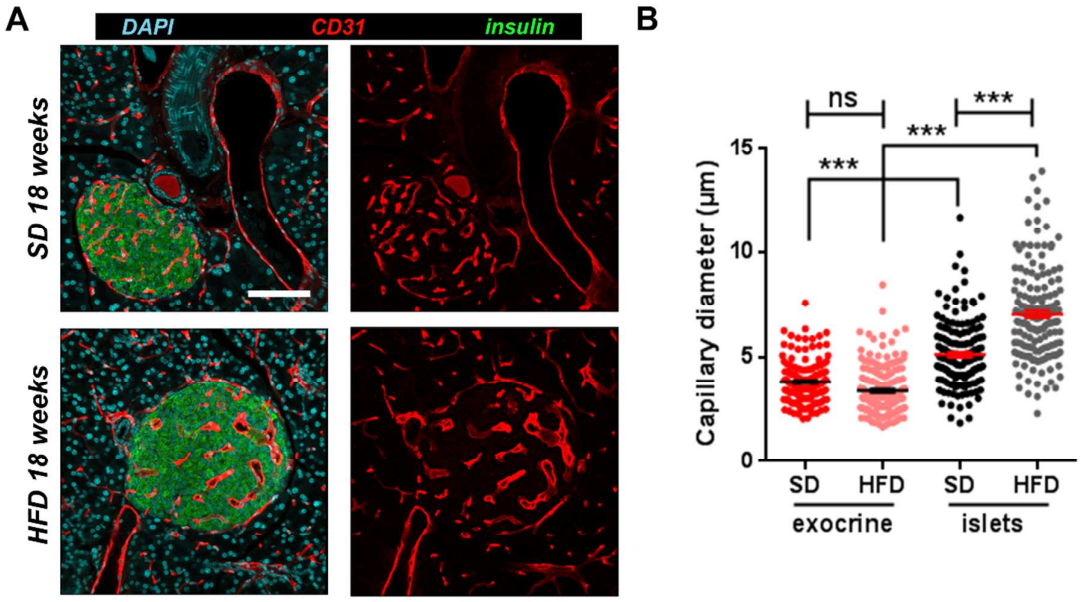

Figure S3

Long-term high fat diet feeding (18 weeks) induces morphological changes to the islet vasculature. A) Representative confocal images of islet vasculature in standard diet (SD) and HFD diet-fed males (scale bar: 100 µm). Z-projections of 12 µm stacks. B) Quantification of capillary diameter show islet vessel dilation at 18 weeks of HFD diet feeding (n = 4 mice per condition; $P<0.0001$ One-way ANOVA). Values represent mean ± SEM.

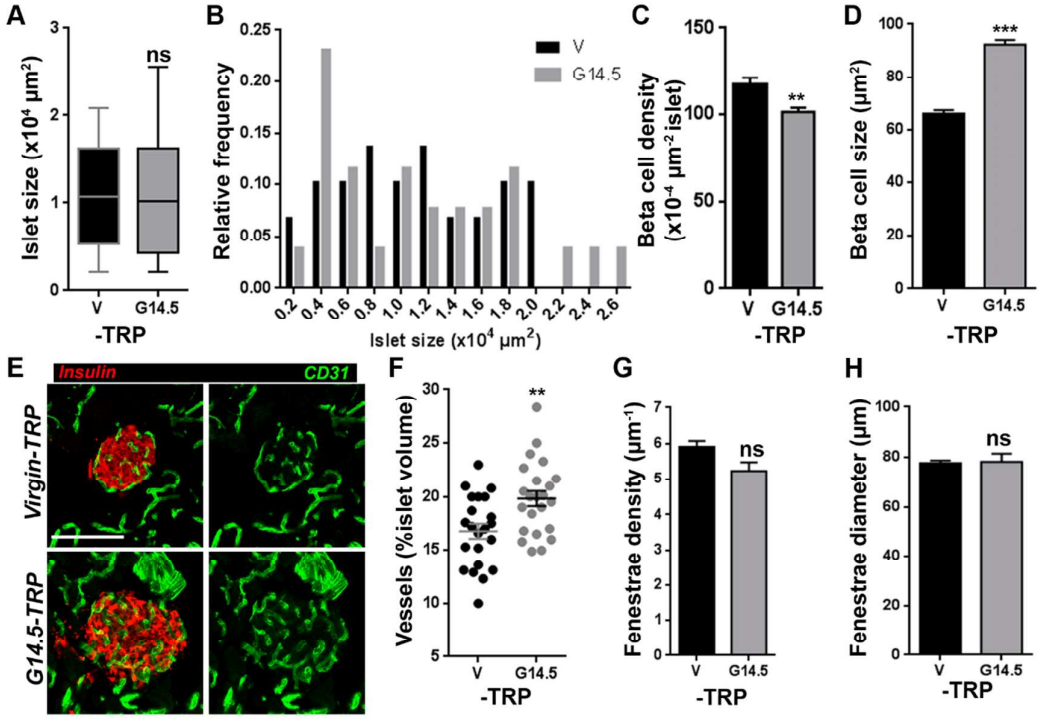

Figure S4

Structural and ultrastructural changes in islets of tryptophan-deprived gestating mice. A) Mean islet size is unchanged by gestation in TRP- conditions (n = 6 mice; P = 0.84, Mann-Whitney test). Values represent mean with range. B) Relative frequency distribution of islet sizes in TRP- conditions shows an increase in the proportion of small and large islets at G14.5. C) Beta cell density in islets, measured as the number of insulin+ cells (presenting a nuclei in cross-section, stained with dapi) per islet surface unit, is reduced at G14.5 –TRP (n = 3 mice, P < 0.01 Mann-Whitney test). D) Beta cells are hypertrophic at G14.5 (n = 6 animals per condition; P < 0.001 Mann-Whitney test). E) Representative confocal images of islet vasculature in virgin and gestating (G14.5) animals fed TRP- diet (scale bar: 100 µm). Z-projections of 11 µm stacks. F) Percentage of islet volume occupied by vessels (n = 6 mice; P<0.01 Student t-test). G) Density of fenestrations shows no variation between virgin and G14.5 fed TRP- diet (n = 2 mice, 22 to 57 µm total endothelium; P = 0.055 Student t-test test). H) Fenestrae diameter measurement shows no variation between virgin and G14.5 fed TRP- diet (n = 2 animals, 25-80 fenestrae; P = 0.87 Student t-test test). Values represent mean ± SEM.

Table S1. Summary of results according to condition. HFD: high fat diet, TRP-: tryptophan deficient diet, ND: not determined, +: increase, ++: large increase; +++: very large increase, 0: unchanged; -: small decrease; - -: large decrease.

	G14.5	HFD 2 weeks	G14.5 TRP-
Glucose intolerance	+	+	+++
Islet size	+++	**0**	**0**
Vessel density	+	**0**	+
Beta cell proliferation	+++	++	**0**
Beta cell size	+++	+++	+++
Islet blood cells velocity	**0**	**0**	**ND**
Vessel lumen perimeter	+	**0**	**ND**
Fenestration diameter	**0**	**0**	**0**
Fenestration density	**0**	**0**	**0**
Permeability in islets	- -	- -	- -
Molecule retention	- -	- -	**ND**
2-NBDG uptake	-	- -	**ND**

SUPPLEMENTAL MOVIES LEGENDS

Movie S1

In vivo diffusion of dextran-FITC molecules from the vasculature into the pancreatic parenchyma. Representative in vivo recordings following i.v. injection of 4-kDa dextran-FITC and 70-kDa dextan-FITC, in exocrine tissue of a virgin female (left), or in an islet of a virgin female (right). Imaging was initiated at the time of i.v. injection of the fluorescent compound. Movie rate: 7 frames/s. Image size: 200×200µm (4-kDa) or 160x160µm (70kDa), single z-plane. Green: FITC. Fluorescence increases in the parenchyma following 4-kDa dextran injection but not following 70-kDa dextran injection.

Movie S2

In vivo diffusion of dextran-FITC molecules from the vasculature in islets of G14.5 gestating animals. Representative in vivo recordings following i.v. injection of 4-kDa dextran-FITC and 70-kDa dextan-FITC, in exocrine tissue of a virgin female (left), or in an islet of a virgin female (middle), and in an islet of a gestating animal (G14.5 stage) (right). Imaging was initiated at the time of i.v. injection of the fluorescent compound. Movie rate: 7 frames/s. Image size: 200×200µm (4-kDa) or 160x160µm (70kDa), single z-plane. Green: FITC. Fluorescence increases in the parenchyma following 4-kDa dextran injection but not following 70-kDa dextran injection.

Movie S3

In vivo diffusion of dextran-FITC molecules from the vasculature in islets of high fat diet-fed animals. Representative in vivo recordings following i.v. injection of 4-kDa dextran-FITC and 70-kDa dextan-FITC in an islet of a standard fed female (left), or in an islet of a 2 weeks female fed HFD for 2 weeks (right). Imaging was initiated at the time of i.v. injection of the fluorescent compound. Movie rate: 7 frames/s. Image size: 200×200µm, single z-plane. Green: FITC. Fluorescence increases in the parenchyma following 4-kDa dextran injection but not following 70-kDa dextran injection.

Movie S4

In vivo diffusion of dextran-FITC molecules from the vasculature islets of tryptophan-deprived animals. Representative in vivo recordings following i.v. injection of 4-kDa dextran-FITC in an islet of a virgin female (left), or in an islet of a gestating animal (G14.5 stage; right), fed with tryptophan-deficient diet. Imaging was initiated at the time of i.v. injection of the fluorescent compound. Movie rate: 7 frames/s. Image size: 400×400µm, single z-plane. Green: FITC.

Movie S5

In vivo 2-NBDG uptake in islets following i.m. injection. Representative in vivo recordings following i.m. injection of 2-NBDG (5 mg/kg) in an islet of a virgin female (left), gestating animal (G14.5 stage; middle), and 2 weeks HFD-fed female (right). Imaging was initiated 1 min post i.m. injection of the fluorescent compound. Total elapsed time: 32.5 min. Image size: 300×300µm, 120µm z-projection. Green: 2-NBDG.

Movie S6

In vivo 2-NBDG uptake in islets following i.v. injection. Representative in vivo recordings following i.v. injection of 2-NBDG (10 mg/kg) in an islet of a virgin female (left), gestating animal (G14.5 stage; middle), and 2 weeks HFD-fed female (right). Imaging was initiated 15s prior to i.v. injection of the fluorescent compound. Total elapsed time: 15.25 min. Image size: 300×300µm, 120µm z-projection. Green: 2-NBDG.

Movie S7

Red blood cells velocity in islets *in vivo*. Representative *in vivo* recordings of blood flow following i.v. injection of 150-kDa dextran-FITC, in an islet of a virgin (left), gestating animal (G14.5 stage, middle), and 2 weeks HFD-fed female (right). Islets are circled. Movie rate: 30 frames/s. Four frames out of 5 have been cut out of the original movies (original movies rate: 150 frames/s). Total elapsed time 6.6 s. Image size: 274×314µm, each movie. Single z-planes. Grey: FITC.